East Asian Journal on Applied Mathematics
doi: 10.4208/eajam.181016.300517f

Vol. 7, No. 4, pp. 852-866
November 2017

A High Order Well-Balanced Finite Volume WENO Scheme for a Blood Flow Model in Arteries

Zhonghua Yao, Gang Li* and Jinmei Gao

School of Mathematics and Statistics, Qingdao University, Qingdao, Shandong 266071, PR China.

Received 18 October 2016; Accepted (in revised version) 30 May 2017.

Abstract. The numerical simulations for the blood flow in arteries by high order accurate schemes have a wide range of applications in medical engineering. The blood flow model admits the steady state solutions, in which the flux gradient is non-zero and is exactly balanced by the source term. In this paper, we present a high order finite volume weighted essentially non-oscillatory (WENO) scheme, which preserves the steady state solutions and maintains genuine high order accuracy for general solutions. The well-balanced property is obtained by a novel source term reformulation and discretisation, combined with well-balanced numerical fluxes. Extensive numerical experiments are carried out to verify well-balanced property, high order accuracy, as well as good resolution for smooth and discontinuous solutions.

AMS subject classifications: 74S10

Key words: Blood flow model, finite volume scheme, WENO scheme, well-balanced property, high order accuracy, source term.

1. Introduction

The numerical simulations for the blood flow in arteries by high order accurate schemes have a wide range of applications in medical engineering [5,8]. The blood flow in arteries can be described by the following one-dimensional blood flow model:

$$\begin{cases} A_t + Q_x = 0, \\ Q_t + \left(\frac{Q^2}{A} + \frac{K}{3\rho\sqrt{\pi}}A^{\frac{3}{2}}\right)_x = \frac{KA}{2\rho\sqrt{\pi}\sqrt{A_0}}(A_0)_x, \end{cases} \tag{1.1}$$

where A is the cross-sectional area (i.e., $A = \pi R^2$ with R being the radius of the vessel), $Q = Au$ represents the discharge, u means the flow velocity, and ρ stands for the blood density. In addition, K denotes the arterial stiffness, and A_0 is the cross section at rest (i.e., $A_0 = \pi R_0^2$ with R_0 being the radius of the vessel, which may be variable in the case of

*Corresponding author. *Email addresses:* yaozhonghuavip@163.com (Z. Yao), gangli1978@163.com (G. Li), gjinmei1979@163.com (J. Gao)

aneurism, stenosis or taper). In general, the original governing equations (1.1) take the following form

$$U_t + F(U)_x = S(A, A_0), \tag{1.2}$$

where U is the solution vector with the corresponding flux $F(U)$, and $S(A, A_0)$ stands for the source term.

The blood flow model (1.1) belongs to the class of hyperbolic equations with source term (also referred as hyperbolic balance laws). The important property of this system is that it usually admits non-trivial steady state solutions, also called mechanical equilibrium:

$$u = 0, \quad A = A_0, \tag{1.3}$$

in which the source term is exactly balanced by the flux gradient. There is a main challenge in the numerical simulation of such balance laws, i.e., the standard numerical schemes may not satisfy the discrete version of this balance exactly at (or near) the steady state, and may introduce spurious oscillations, when the mesh is not extremely refined. However, the mesh refinement approach is not practical for the high dimensional problems. Therefore, well-balanced schemes [6] are specially designed to preserve exactly these steady state solutions up to the machine accuracy for the purpose of saving the computational cost. In addition, the well-balanced schemes can capture small perturbations on relatively coarse meshes [17]. We can refer to [11] for more information about the well-balanced schemes.

In the last few years, there have been many interesting attempts proposed in the literature to derive well-balanced schemes for the blood flow model. For instance, based on the conservative governing equations [1,2,15] and the hydrostatic reconstruction, Delestre and Lagrée [3] presented a well-balanced finite volume scheme for the blood flow model. Recently, Müller et al. [10] constructed a well-balanced high order finite volume scheme for the blood flow in elastic vessels with varying mechanical properties. And Murillo et al. [9] designed an energy-balanced approximate solver for the blood flow model with upwind discretisation for the source term. More recently, Wang et al. [16] have presented a high order well-balanced finite difference weighted essentially non-oscillatory (WENO) scheme.

During the past few decades, high order finite volume WENO schemes have gained great attentions in solving hyperbolic conservation laws [12]. Several advantages of the WENO schemes, including its accuracy and essentially non-oscillatory property, make it useful for a wide range of applications.

The main objective of this paper is to present a high order accurate finite volume well-balanced WENO scheme for the blood flow model in arteries. To achieve the well-balanced property, we firstly reformulate the source terms in an equivalent form by using the steady state (1.3). Then, we apply well-balanced numerical fluxes accordingly.

In Section 2, we present a novel high order well-balanced finite volume WENO scheme. Section 3 contains extensive numerical results to demonstrate the behavior of our well-balanced WENO scheme for the blood flow model, verifying high order accuracy, the well-balanced property, and good resolution for smooth and discontinuous solutions. Some conclusions are given in Section 4.

2. Well-Balanced WENO Scheme

In this section, we design a high order accurate well-balanced finite volume WENO scheme for the blood flow model satisfying the steady state solutions (1.3).

2.1. Notations and WENO reconstruction

We firstly introduce some notations and the standard WENO reconstruction which will be applied later. In one space dimension, the computational domain is divided into cells $I_j = [x_{j-\frac{1}{2}}, x_{j+\frac{1}{2}}]$ with $\Delta x = x_{j+\frac{1}{2}} - x_{j-\frac{1}{2}}$ being the mesh size. The usual notation $\{u\} = (u^+ + u^-)/2$ is used to represent the arithmetic average of the function u at the cell interfaces.

Under the framework of the finite volume schemes for the hyperbolic balance laws (1.2), our computational variables are $\overline{U}_j(t)$, which approximate the cell averages $\overline{U}(x_j,t) = \frac{1}{\Delta x}\int_{I_j} U(x,t)\,\mathrm{d}x$. The conservative finite volume WENO scheme for the hyperbolic balance laws can be given by

$$\frac{\mathrm{d}}{\mathrm{d}t}\overline{U}_j(t) + \frac{1}{\Delta x}\left(\widehat{F}_{j+\frac{1}{2}} - \widehat{F}_{j-\frac{1}{2}}\right) = \frac{1}{\Delta x}\int_{I_j} S\mathrm{d}x, \tag{2.1}$$

with $\widehat{F}_{j+\frac{1}{2}} = f(U^-_{j+\frac{1}{2}}, U^+_{j+\frac{1}{2}})$ being the numerical flux. The simplest numerical flux is the well-known Lax-Friedrichs flux

$$f(a,b) = \frac{1}{2}\big(F(a) + F(b) - \alpha(b-a)\big), \tag{2.2}$$

where $\alpha = \max_x |\lambda(U)|$ with $\lambda(U)$ being the eigenvalues of the Jacobian matrix $F'(U)$, and the maximum is taken over the whole region. $U^-_{j+\frac{1}{2}}$ and $U^+_{j+\frac{1}{2}}$ are the high order pointwise approximations to $U(x_{j+\frac{1}{2}},t)$ on left and right of the cell interface $x_{j+\frac{1}{2}}$ respectively. They are computed through the neighboring cell average values by a high order WENO reconstruction procedure. Basically, for a $(2k-1)$-th order WENO scheme, we firstly compute k reconstructed boundary values $U^{(k),\pm}_{j+\frac{1}{2}}$ corresponding to different candidate stencils. Then by providing each value a nonlinear weight which indicates the smoothness of the corresponding stencil, we define the $(2k-1)$-th order WENO reconstruction $U^{\pm}_{j+\frac{1}{2}}$ as a convex combination of all these k reconstructed values. Eventually, the WENO reconstruction can be written out as:

$$U^-_{j+\frac{1}{2}} = \sum_{r=-k+1}^{k-1} w_r \overline{U}_{j+r}, \qquad U^+_{j+\frac{1}{2}} = \sum_{r=-k+2}^{k} \widetilde{w}_r \overline{U}_{j+r} \tag{2.3}$$

the coefficients w_r and $\widetilde{w}_r$ depend nonlinearly on the smoothness indicators involving the cell averages $\overline{U}$. For hyperbolic systems of conservation laws, we usually apply the local characteristic decomposition procedure, which is more robust than a component by component version. The complete algorithm can be found in [7, 12].

2.2. Reformulation of the equations

Firstly, in order to achieve the well-balanced property, we split the source term into two terms, *i.e.*, $\frac{KA}{2\rho\sqrt{\pi}\sqrt{A_0}}(A_0)_x = \frac{K}{\rho\sqrt{\pi}}(A-A_0)(\sqrt{A_0})_x + \frac{K}{3\rho\sqrt{\pi}}(A_0^{\frac{3}{2}})_x$. Therefore, the original system (1.1) can be rewritten as

$$\begin{cases} A_t + Q_x = 0, \\ Q_t + \left(\frac{Q^2}{A} + \frac{K}{3\rho\sqrt{\pi}}A^{\frac{3}{2}}\right)_x = \frac{K}{\rho\sqrt{\pi}}(A-A_0)(\sqrt{A_0})_x + \frac{K}{3\rho\sqrt{\pi}}\left(A_0^{\frac{3}{2}}\right)_x, \end{cases} \tag{2.4}$$

which can also be denoted in a compact vector form

$$U_t + F(U)_x = S,$$

where $U = (A,\ Q)^T$, $F(U) = (Q,\ \frac{Q^2}{A} + \frac{K}{3\rho\sqrt{\pi}}A^{\frac{3}{2}})^T$, $S = (0,\ \frac{K}{\rho\sqrt{\pi}}(A-A_0)(\sqrt{A_0})_x + \frac{K}{3\rho\sqrt{\pi}}(A_0^{\frac{3}{2}})_x)^T$, with the superscript T denoting the transpose.

2.3. Novel source term approximation

For the approximation of the source term $S^{[2]}$ in the second equation, we can decompose its integral as

$$\frac{1}{\Delta x}\int_{I_j} S^{[2]}\mathrm{d}x = \frac{1}{\Delta x}\frac{K}{\rho\sqrt{\pi}}\int_{I_j}(A-A_0)\left(\sqrt{A_0}\right)_x \mathrm{d}x + \frac{1}{\Delta x}\frac{K}{3\rho\sqrt{\pi}}\left(\left(A_0^{\frac{3}{2}}\right)_{j+\frac{1}{2}} - \left(A_0^{\frac{3}{2}}\right)_{j-\frac{1}{2}}\right). \tag{2.5}$$

Then we take the following numerical approximation

$$\frac{1}{\Delta x}\int_{I_j} S^{[2]}\mathrm{d}x \approx \frac{1}{\Delta x}\frac{K}{\rho\sqrt{\pi}}\int_{I_j}(A-A_0)\left(\sqrt{A_0}\right)_x \mathrm{d}x + \frac{1}{\Delta x}\frac{K}{3\rho\sqrt{\pi}}\left(\left\{A_0^{\frac{3}{2}}\right\}_{j+\frac{1}{2}} - \left\{A_0^{\frac{3}{2}}\right\}_{j-\frac{1}{2}}\right), \tag{2.6}$$

where $(A_0^{\frac{3}{2}})_{j\pm\frac{1}{2}}$ is replaced by $\{A_0^{\frac{3}{2}}\}_{j\pm\frac{1}{2}} = \frac{1}{2}((A_0^{\frac{3}{2}})^+_{j\pm\frac{1}{2}} + (A_0^{\frac{3}{2}})^-_{j\pm\frac{1}{2}})$, and the integration in the first term on the right hand side can be obtained by the standard Gaussian quadrature rule.

2.4. Well-balanced numerical fluxes

Finally, we modify the numerical flux $\widehat{F}_{j+\frac{1}{2}}$ to design a well-balanced WENO scheme. The term $\alpha(b-a)$ in the Lax-Friedrichs flux (2.2) leads to the numerical viscosity term, which is essential for this nonlinear hyperbolic conservation laws. However, the well-balanced property of the resulting scheme will be destroyed by them at the steady state. Therefore, we propose to modify the original numerical flux as follows

$$\widehat{F}_{j+\frac{1}{2}} = \frac{1}{2}\left[F\left(U^+_{j+\frac{1}{2}}\right) + F\left(U^-_{j+\frac{1}{2}}\right) - \alpha_j\left(\widetilde{U}^+_{j+\frac{1}{2}} - \widetilde{U}^-_{j+\frac{1}{2}}\right)\right], \tag{2.7}$$

with $\widetilde{U}$ being given by

$$\widetilde{U} = (A-A_0,\ Q)^T,$$

which ensures that $\widetilde{U} = constant$ and the effect of the viscosity terms $\widetilde{U}^{+}_{j+\frac{1}{2}} - \widetilde{U}^{-}_{j+\frac{1}{2}}$ disappears at the steady state. Therefore, the effect of these viscosity terms becomes zero and the original numerical flux now reduces to a simple form

$$\widehat{F}_{j+\frac{1}{2}} = \frac{1}{2}\left[F\left(U^{+}_{j+\frac{1}{2}}\right) + F\left(U^{-}_{j+\frac{1}{2}}\right)\right]. \tag{2.8}$$

2.5. Well-balanced scheme

All of these together lead to a well-balanced finite volume WENO scheme for the blood flow model in arteries, as outlined in the following proposition.

Proposition 2.1. *For the blood flow model* (1.1)*, the semi-discrete scheme* (2.1)*, combined with* (2.6) *and* (2.7)*, are well-balanced for the steady state solutions* (1.3).

Proof. At the steady state (1.3), we have

$$u = 0, \quad A = A_0.$$

It is obvious to conclude that the well-balanced property holds for the first equation, as both the numerical flux and the source term approximation in these equations become zero. For the second equation, the source term approximation becomes

$$\frac{1}{\Delta x}\int_{I_j} S^{[2]}\mathrm{d}x \approx \frac{1}{\Delta x}\frac{K}{3\rho\sqrt{\pi}}\left(\left\{A_0^{\frac{3}{2}}\right\}_{j+\frac{1}{2}} - \left\{A_0^{\frac{3}{2}}\right\}_{j-\frac{1}{2}}\right). \tag{2.9}$$

Since $u = 0$ leading to $Q = Au = 0$, so the flux term $F^{[2]} = \frac{Q^2}{A} + \frac{K}{3\rho\sqrt{\pi}}A^{\frac{3}{2}}$ reduces to $\frac{K}{3\rho\sqrt{\pi}}A^{\frac{3}{2}}$, and its numerical approximation takes the following form:

$$\frac{1}{\Delta x}\left(\widehat{F}^{[2]}_{j+\frac{1}{2}} - \widehat{F}^{[2]}_{j-\frac{1}{2}}\right) = \frac{1}{\Delta x}\frac{K}{3\rho\sqrt{\pi}}\left(\left\{A^{\frac{3}{2}}\right\}_{j+\frac{1}{2}} - \left\{A^{\frac{3}{2}}\right\}_{j-\frac{1}{2}}\right). \tag{2.10}$$

From (2.9) and (2.10) and based on the fact that $A = A_0$, we can conclude that the flux and source term approximations balance each other, which indicates that our scheme can preserve the well-balanced property. As a consequence, this finishes the proof. □

For the temporal discretisation, high order total variation diminishing (TVD) Runge-Kutta methods [13] can be taken into consideration. In the numerical section of this paper, we apply the third order Runge-Kutta method:

$$\begin{aligned} U^{(1)} &= U^n + \Delta t\mathscr{F}(U^n), \\ U^{(2)} &= \frac{3}{4}U^n + \frac{1}{4}\left(U^{(1)} + \Delta t\mathscr{F}(U^{(1)})\right), \\ U^{n+1} &= \frac{1}{3}U^n + \frac{2}{3}\left(U^{(2)} + \Delta t\mathscr{F}(U^{(2)})\right), \end{aligned} \tag{2.11}$$

with $\mathscr{F}(U)$ being the spatial operator.

Table 1: L^1 errors and numerical orders of accuracy for the Section 3.1.

N	A		Q	
	L^1 error	Order	L^1 error	Order
100	3.3556E-04		2.7724E-03	
200	2.2322E-05	3.91	1.9630E-04	3.82
400	8.8296E-07	4.66	7.9830E-06	4.62
800	2.9166E-08	4.92	3.3609E-07	4.57
1600	8.8039E-10	5.05	1.0287E-08	5.03

3. Numerical Results

In this section, we carry out extensive numerical experiments to demonstrate the performances of a fifth-order ($k = 3$) finite volume well-balanced WENO scheme. The CFL number is taken as 0.6 for all the computations.

3.1. To test the order of accuracy

We apply this example to test the order of accuracy of the resulting scheme. We take the following initial conditions:

$$A(x,0) = \sin^2(\pi x), \quad Q(x,0) = \sin(\pi x) + \cos(\pi x) \quad \text{and} \quad A_0(x) = \cos^2(\pi x),$$

on a computational domain $[0,2]$ based on the following parameters: $K = 1 \times 10^8\, Pa/m$, $\rho = 1060\ kg/m^3$.

We impose this problem with periodic boundary conditions at the two endpoints. Then, we solve this example up to $t = 0.1$ s and get reference solutions on a mesh with 2000 cells. We present the errors and the order of accuracy in Table 1. As expected, we recover fifth order errors.

3.2. The ideal tourniquet

This example is similar to the dam break problem for shallow water equations [4]. Herein, we consider the analogous problem in blood flow model: a tourniquet is applied and we remove it instantaneously. And we deal with the following initial conditions

$$A(x,0) = \begin{cases} \pi R_L^2 & \text{if } x \le 0, \\ \pi R_R^2 & \text{otherwise,} \end{cases} \quad \text{and} \quad Q(x,0) = 0,$$

on a computational domain $[-L, L]$ based on the following parameters: $K = 1. \times 10^7\, Pa/m$, $\rho = 1060\ kg/m^3$, $R_L = 5 \times 10^{-3}\, m$, $R_R = 4 \times 10^{-3}\, m$, $L = 0.04\ m$.

We impose this problem with transmissive boundary conditions at the two endpoints. Then, we solve this example on a mesh with 200 cells up to $t = 0.005$ s and present the numerical solutions against the exact ones in Fig. 1. It is clear that the numerical results fit well with the exact ones and keep steep discontinuity transitions at the same time.

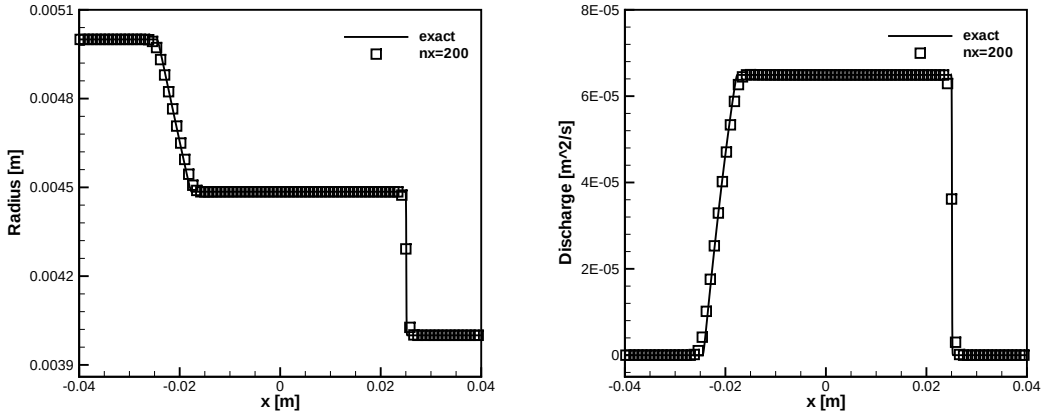

Fig. 1: The numerical solutions of the ideal tourniquet problem in Section 3.2 on a mesh with 200 cells at $t = 0.005$ s. Radius (left) and discharge (right).

3.3. Wave equation

Then, the following quasi-stationary test case has been proposed by Delestre and Lagrée [3]. It is chosen to demonstrate the capability of the proposed scheme for computations on the perturbation of steady state solutions.

With initial conditions $R(x,0) = \Phi(x)$, $u(x,0) = 0$, we obtain the following exact solutions:

$$\begin{cases} R(x,t) &= R_0 + \frac{\epsilon}{2}[\Phi(x - C_0 t) + \Phi(x + C_0 t)], \\ u(x,t) &= -\frac{\epsilon}{2}\frac{C_0}{R_0}[-\Phi(x - C_0 t) + \Phi(x + C_0 t)], \end{cases}$$

with the Moens Korteweg wave velocity

$$C_0 = \sqrt{\frac{K\sqrt{A_0}}{2\rho\sqrt{\pi}}} = \sqrt{\frac{KR_0}{2\rho}}.$$

Herein, we apply the following initial data:

$$A(x,0) = \begin{cases} \pi R_0^2 & \text{if } x \in \left[0, \frac{40L}{100}\right] \cup \left[\frac{60L}{100}, L\right], \\ \pi R_0^2 \left[1 + \epsilon \sin\left(\pi \frac{x - 40L/100}{20L/100}\right)\right]^2 & \text{if } x \in \left[\frac{40L}{100}, \frac{60L}{100}\right], \end{cases}$$

and $Q(x,0) = 0$ on a computational domain $[0, L]$. The following parameters have been used for this example: $\epsilon = 5 \times 10^{-3}$, $K = 10^8\, Pa/m$, $\rho = 1060\, kg/m^3$, $R_0 = 4 \times 10^{-3}\, m$ and $L = 0.16\, m$.

We impose this problem with transmissive boundary conditions at the two endpoints. Then, we show the numerical solutions on a mesh with 200 cells at $t = 0.002s$, $0.004s$, and $0.006s$ against the exact solutions, respectively, in Fig. 2. The figures strongly suggest that the numerical solutions agree well with the exact ones.

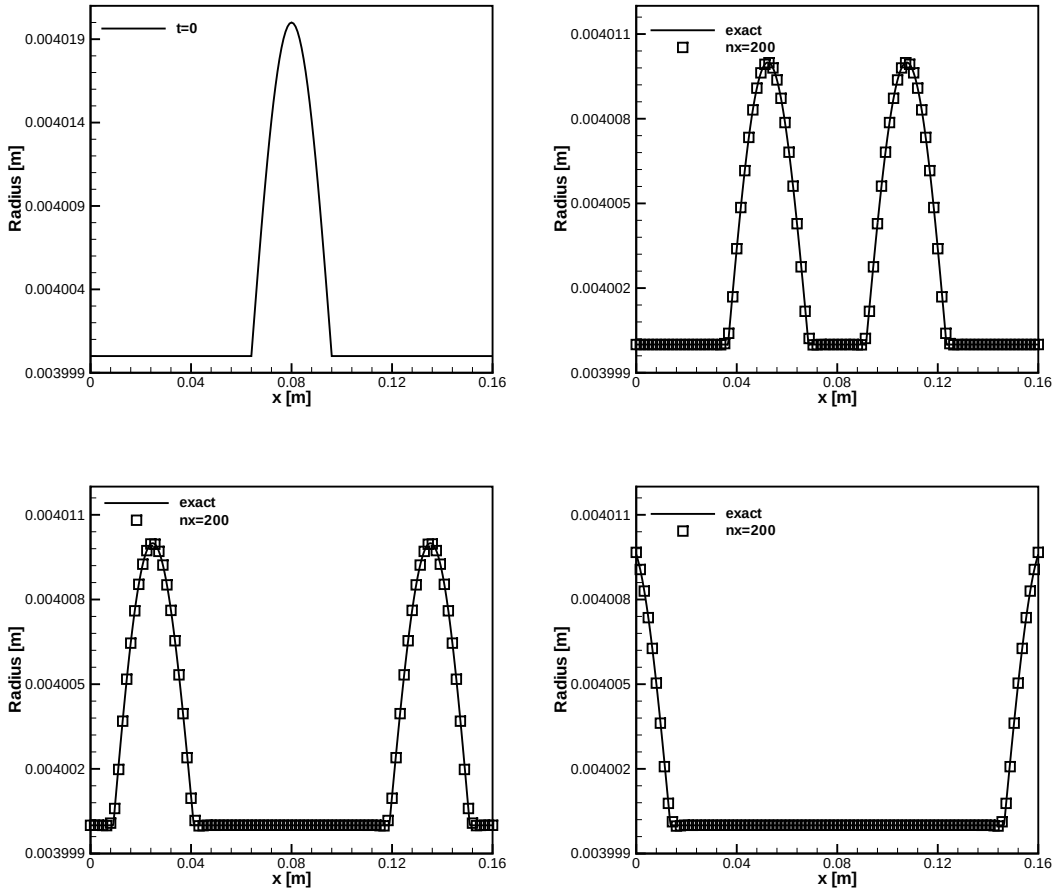

Fig. 2: The numerical solutions of the wave equation problem in Section 3.3 on a mesh with 200 cells. Radius at time $t = 0s$ (upper left), $t = 0.002s$ (upper right), $t = 0.004s$ (lower left), and $t = 0.006s$ (lower right), respectively.

3.4. The man at eternal rest

The purpose of this example is to verify that the proposed scheme indeed maintains the well-balanced property. Herein, we consider a configuration with no flow and with a change of radius $R_0(x)$, this is the case for a dead man with an aneurism. Therefore, for the initial conditions, the section of the artery is not constant with the following form

$$R(x,0) = R_0(x) = \begin{cases} \widetilde{R} & \text{if } x \in [0, x_1] \cup [x_4, L], \\ \widetilde{R} + \frac{\Delta R}{2}\left[\sin\left(\frac{x-x_1}{x_2-x_1}\pi - \frac{\pi}{2}\right) + 1\right] & \text{if } x \in [x_1, x_2], \\ \widetilde{R} + \Delta R & \text{if } x \in [x_2, x_3], \\ \widetilde{R} + \frac{\Delta R}{2}\left[\cos\left(\frac{x-x_3}{x_4-x_3}\pi\right) + 1\right] & \text{if } x \in [x_3, x_4], \end{cases}$$

Table 2: L^1 and L^∞ errors for different precisions for the man at eternal rest.

Precision	L^1 error		L^∞ error	
	A	Q	A	Q
Single	3.32e-07	3.83e-07	3.57e-07	2.75e-07
Double	2.31e-16	4.18e-16	2.31e-15	3.44e-16
Quadruple	7.82e-31	4.64e-32	2.28e-33	3.44e-31

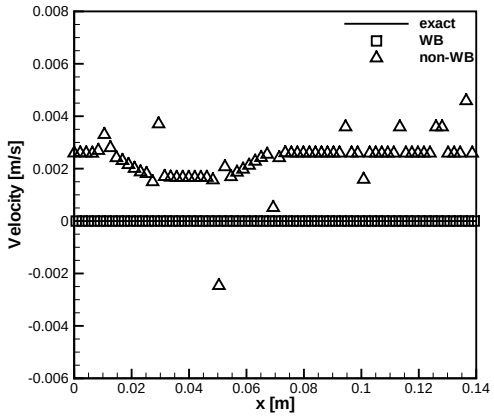

Fig. 3: The man at eternal rest problem in Section 3.4 on a mesh with 200 cells at $t = 5s$. The result of the well-balanced (denoted by WB) scheme with 200 and 2000 cells, and that of the non-well-balanced (denoted by non-WB) scheme with 200 cells.

on a computational domain $[0, L]$ with $\widetilde{R} = 4 \times 10^{-3}\, m, \Delta R = 10^{-3}\, m$, $K = 10^8\, Pa/m$, $\rho = 1060\, kg/m^3$, $L = 0.14\, m$, $x_1 = 10^{-2}\, m$, $x_2 = 3.05 \times 10^{-2}\, m$, $x_3 = 4.95 \times 10^{-2}\, m$ and $x_4 = 7 \times 10^{-2}\, m$. In addition, the initial velocity is zero. We impose this problem with transmissive boundary conditions at the two endpoints. Then, we compute this example up to $t = 5\, s$.

In order to show that the well-balanced property is maintained up to machine round-off error, tests are run using single, double and quadruple precisions, respectively. The L^1 and L^∞ errors calculated for A and Q are presented in Table 2. It can be clearly seen that the L^1 and L^∞ errors are all at the level of round-off error associated with different precisions, which verify that the current scheme maintains the well-balanced property as expected.

In Fig. 3, we present the velocity at $t = 5\, s$ on a mesh with 200 cells against a reference solution obtained with a much refined mesh with 2000 cells. In addition, we run the same numerical test using the non-well-balanced WENO schemes, with a straightforward integration of the source term, and show their results in Fig. 3 for comparison. It is obvious that the results of the well-balanced WENO scheme are in good agreement with the reference solutions for the case, while the non-well-balanced WENO scheme fails to capture the small perturbation with 200 cells.

3.5. Propagation of a pulse to an expansion

Firstly, we test the case of a pulse in a section $R_{_R}$ passing through an expansion: $A_L > A_R$, taking the following parameters: $K = 1 \times 10^8\, Pa/m$, $L = 0.16\, m, \rho = 1060\, kg/m^3$, $R_{_L} = 5 \times 10^{-3}\, m$, $R_{_R} = 4 \times 10^{-3}\, m$, $\Delta R = 1 \times 10^{-3}\, m$. We take a decreasing shape on a rather small scale:

$$R_0(x) = \begin{cases} R_{_R} + \Delta R & \text{if } x \in [0, x_1], \\ R_{_R} + \frac{\Delta R}{2}\Big[1 + \cos\Big(\frac{x - x_1}{x_2 - x_1}\pi\Big)\Big] & \text{if } x \in [x_1, x_2], \\ R_{_R} & \text{else,} \end{cases}$$

with $x_1 = 19L/40,\ x_2 = L/2$. As initial conditions, we consider a fluid at rest $Q(x,0) = 0\, m^3/s$ and the following perturbation of radius:

$$R(x,0) = \begin{cases} R_0(x)\big[1 + \epsilon \sin\big(\frac{100}{20L}\pi(x - \frac{65L}{100})\big)\big] & \text{if } x \in \big[\frac{65L}{100}, \frac{85L}{100}\big], \\ R_0(x) & \text{else,} \end{cases}$$

with $\epsilon = 5.0 \times 10^{-3}$. And we impose this problem with transmissive boundary conditions at the two endpoints.

We present the numerical results against the reference solutions at $t = 0.002\, s$ and $t = 0.006\, s$ in Fig. 4. It is obvious that the numerical solutions are in good agreement with the reference ones and are comparable with those in [3].

3.6. Propagation of a pulse from an expansion

Then, we consider a pulse propagating from an expansion. Therefore, the parameters are the same as in the Section 3.5, only the initial radius is changed:

$$R(x,0) = \begin{cases} R_0(x)\big[1 + \epsilon \sin\big(\frac{100}{20L}\pi\big(x - \frac{15L}{100}\big)\big)\big] & \text{if } x \in \big[\frac{15L}{100}, \frac{35L}{100}\big], \\ R_0(x) & \text{else,} \end{cases}$$

with $\epsilon = 5.0 \times 10^{-3}$.

In Fig. 5, we demonstrate the numerical results against the reference solutions at $t = 0.002\, s$ and $t = 0.006\, s$. Similarly, the numerical solutions fit well with the reference ones and are comparable with those in [3].

3.7. Wave damping

In the last test part, we look at the viscous damping term in the linearized momentum equation. This is an analogue of the Womersley [14] problem, and we consider a periodic signal at the inflow with a constant section at rest. We consider the following model coupled with a linear friction term

$$\begin{cases} A_t + Q_x = 0, \\ Q_t + \Big(\frac{Q^2}{A} + \frac{K}{3\rho\sqrt{\pi}}A^{\frac{3}{2}}\Big)_x = \frac{KA}{\rho\sqrt{\pi}}(\sqrt{A_0})_x - C_f\frac{Q}{A}, \end{cases} \tag{3.1}$$

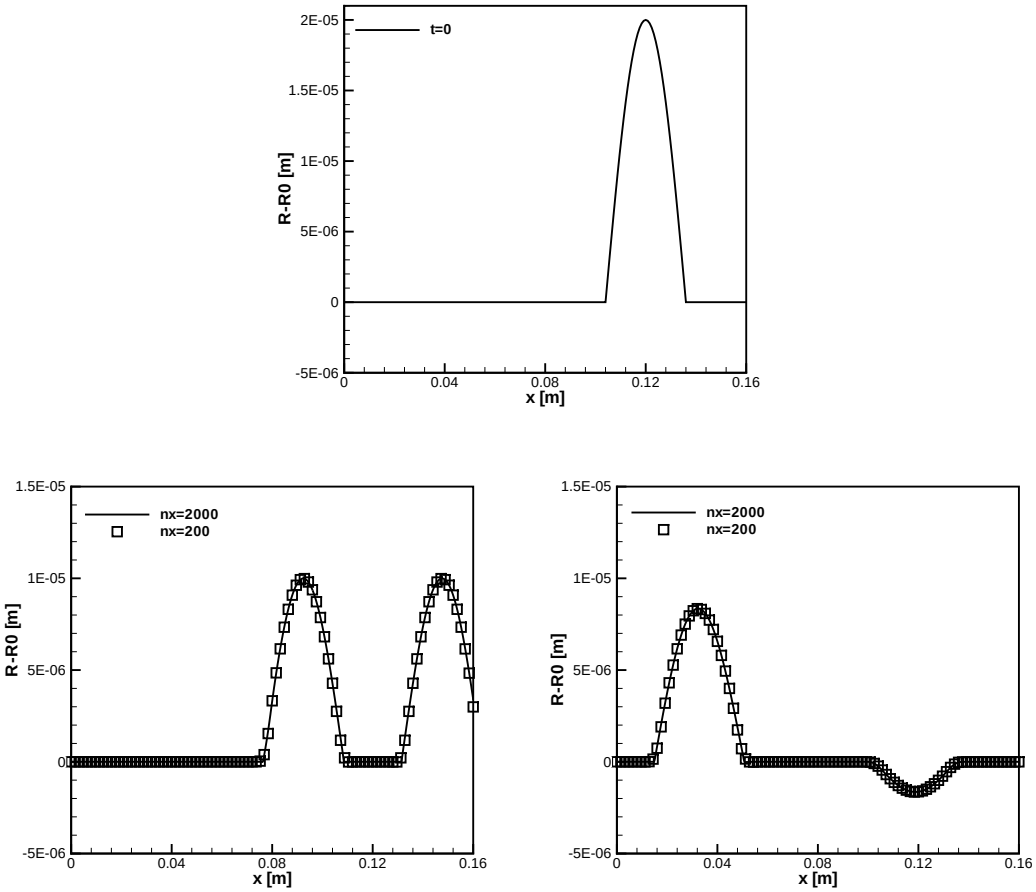

Fig. 4: The numerical solutions of the propagation of a pulse to an expansion in Section 3.5 on a mesh with 200 cells. The errors $R-R_0$ at $t=0s$ (upper), $t=0.002s$ (lower left) and $t=0.006s$ (lower right).

where $C_f = 8\pi\nu$ with ν being the blood viscosity. We consider this example on a computational domain $[0,3]$ subject to the given initial conditions

$$\begin{cases} A(x,0) = \pi R_0^2, \\ Q(x,0) = 0, \end{cases}$$

accompanied by the following parameters: $K = 1\times 10^8\, Pa/m$, $\rho = 1060\, kg/m^3$, $R_0 = 4\times 10^{-}3\, m$. We solve this example up to $t = 25\, s$.

Subsequently, we obtain a damping wave in the domain [3]

$$Q(t,x) = \begin{cases} 0 & \text{if } k_r x > \omega t, \\ Q_{\text{amp}} \sin(\omega t - k_r x) e^{k_i x} & \text{if } k_r x \le \omega t, \end{cases} \tag{3.2}$$

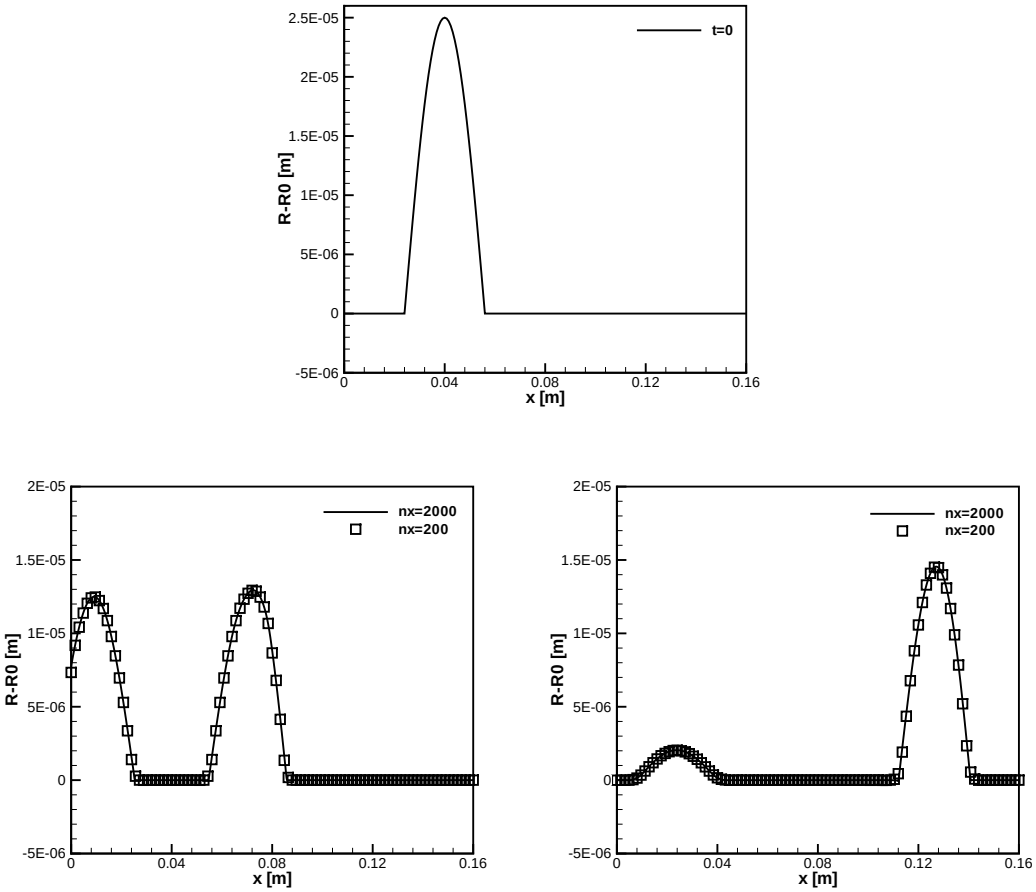

Fig. 5: The numerical solutions of the propagation of a pulse from an expansion in Section 3.6 on a mesh with 200 cells. The errors $R-R_0$ at $t=0s$ (upper), $t=0.002s$ (lower left) and $t=0.006s$ (lower right).

with

$$k_r = \left[\frac{\omega^4}{c_0^4} + \left(\frac{\omega C_f}{\pi R_0^2 c_0^2}\right)^2\right]^{\frac{1}{4}} \cos\left(\frac{1}{2}\arctan\left(-\frac{C_f}{\pi R_0^2 \omega}\right)\right),$$

$$k_i = \left[\frac{\omega^4}{c_0^4} + \left(\frac{\omega C_f}{\pi R_0^2 c_0^2}\right)^2\right]^{\frac{1}{4}} \sin\left(\frac{1}{2}\arctan\left(-\frac{C_f}{\pi R_0^2 \omega}\right)\right),$$

$$\omega = 2\pi/T_{\text{pulse}} = 2\pi/0.5\,s,$$

$$c_0 = \sqrt{\frac{K\sqrt{A_0}}{2\rho\sqrt{\pi}}} = \sqrt{\frac{KR_0}{2\rho}}.$$

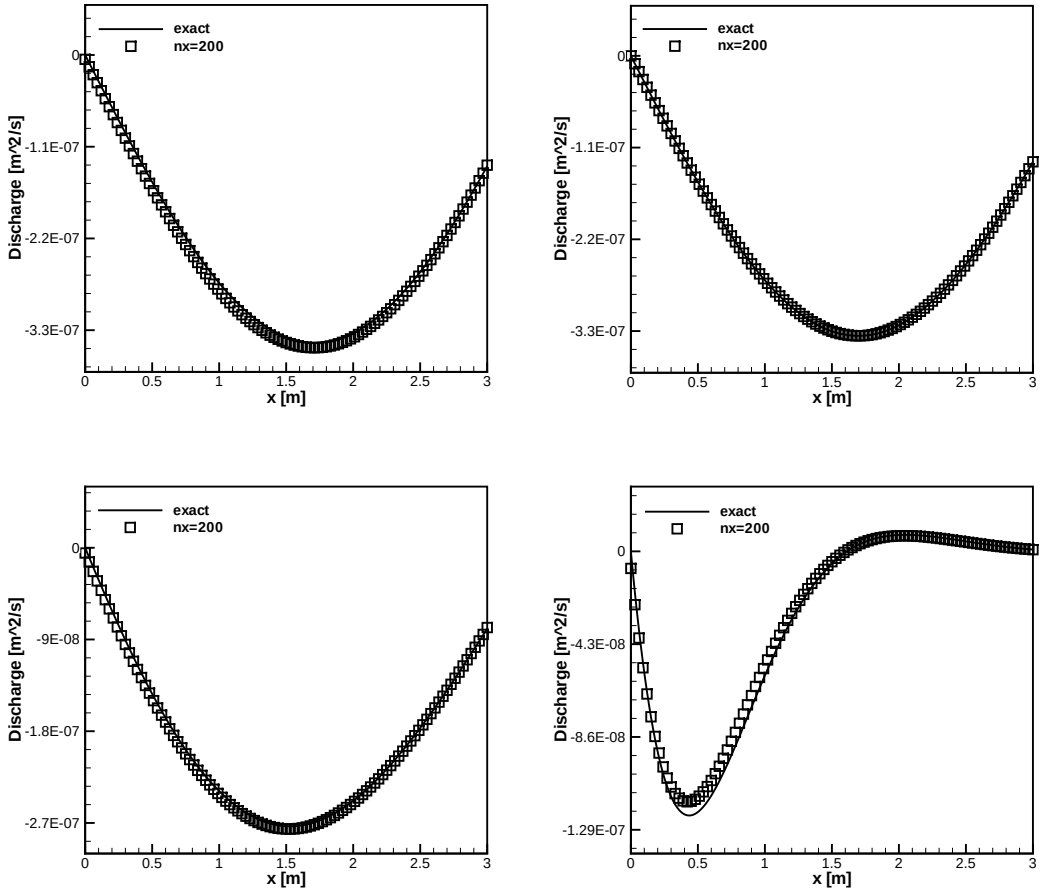

Fig. 6: The numerical solutions of the wave damping problem in Section 3.7 on a mesh with 200 cells at $t = 25s$. The damping of a discharge wave with $C_f = 0$ (upper left), $C_f = 0.000022$ (upper right), $C_f = 0.000202$ (lower left) and $C_f = 0.005053$ (lower right). The friction term has been treated with the explicit method.

For the boundary conditions, we impose the incoming discharge

$$Q_b(t) = Q_{\text{amp}} \sin(\omega t)\, m^3/s,$$

at $x = 0\,m$ with $Q_{\text{amp}} = 3.45 \times 10^{-7}\, m^3/s$ being the amplitude of the inflow discharge. As the flow is subcritical, the discharge is imposed at the outflow boundary, thanks to (3.2) at the right boundary $x = 3\,m$.

We present the numerical results against the exact solutions at $t = 25\,s$ with different C_f in Fig. 6. The numerical solutions are in good agreement with the exact solutions and are comparable with those in [3].

4. Conclusions

In this paper, we present a high order well-balanced finite volume WENO scheme to solve the blood flow model in arteries. A special splitting of the source term allows us to construct specific approximations to the source term. With the help of well-balanced numerical fluxes, the resulting WENO scheme maintains the well-balanced property for steady state solutions, and at the same time keeps its original high order accuracy and essentially non-oscillatory property for general solutions. Extensive numerical examples are given to demonstrate the well-balanced property, high order accuracy, and steep shock transitions of the proposed numerical scheme.

Acknowledgments

The research of the second author is supported by the Natural Science Foundation of P.R. China (11201254,11401332,11771228) and the Project for Scientific Plan of Higher Education in Shandong Province of P.R. China (J12LI08). This work was partially performed at the State Key Laboratory of Science/Engineering Computing of P.R. China by virtue of the computational resources of Professor Li Yuan's group. The second author is also thankful to Professor Li Yuan for his kind invitation.

References

[1] N. Cavallini, V. Caleffi and V. Coscia, *Finite volume and WENO scheme in one-dimensional vascular system modelling*, Comput. Math. Appl. **56**, 2382-2397 (2008).
[2] N. Cavallini and V. Coscia, *One-dimensional modelling of venous pathologies: Finite volume and WENO schemes*, In Advances in Mathematical Fluid Mechanics, Rannacher R, Sequeira A (eds). Springer: Berlin Heidelberg, 2010.
[3] O. Delestre and P.Y. Lagrée, *A 'well-balanced' finite volume scheme for blood flow simulation,* Int. J. Numer. Meth. Fl. **72**, 177-205 (2013).
[4] O. Delestre, C. Lucas, P.A. Ksinant, F. Darboux, C. Laguerre, T.N.T. Vo, F. James and S. Cordier, *SWASHES: A compilation of Shallow Water Analytic Solutions for Hydraulic and Environmental Studies*, Int. J. Numer. Meth. Fl. **72**, 269-300 (2013).
[5] L. Formaggia, D. Lamponi, M. Tuveri and A. Veneziani, *Numerical modeling of 1D arterial networks coupled with a lumped parameters description of the heart*, Comput. Method Biomech. Biomed. Engin. **9**, 273-288 (2006).
[6] J.M. Greenberg and A.Y. LeRoux, *A well-balanced scheme for the numerical processing of source terms in hyperbolic equations*, SIAM J. Numer. Anal. **33**, 1-16 (1996).
[7] G. Jiang and C.W. Shu, *Efficient implementation of weighted ENO schemes*, J. Comput. Phys. **126**, 202-228 (1996).
[8] V.B. Kolachalama, N.W. Bressloff, P.B. Nair and C.P. Shearman, *Predictive Haemodynamics in a one-dimensional human carotid artery bifurcation. Part I: Application to stent design*, IEEE T. Bio-Med. Eng. **54**, 802-812 (2007).
[9] J. Murillo and P. García-Navarro, *A Roe type energy balanced solver for 1D arterial blood flow and transport*, Comput. Fluids **117**, 149-167 (2015).

[10] L.O. Müller, C. Parés and E.F. Toro, *Well-balanced high-order numerical schemes for one-dimensional blood flow in vessels with varying mechanical properties*, J. Comput. Phys. **242**, 53-85 (2013).
[11] S. Noelle, Y. L. Xing and C.W. Shu, *High-order well-balanced schemes*, In: Numerical Methods for Balance Laws (G. Puppo and G. Russo eds). Quaderni di Matematica (2010).
[12] C.W. Shu, *Essentially non-oscillatory and weighted essentially non-oscillatory schemes for hyperbolic conservation laws*, In A. Quarteroni, editor, *Advanced Numerical Approximation of Nonlinear Hyperbolic Equations*, pp. 325-432. Lecture Notes in Mathematics, volume 1697, Springer, 1998.
[13] C.W. Shu and S. Osher, *Efficient implementation of essentially non-oscillatory shock-capturing schemes*, J. Comput. Phys. **77**, 439-4718 (1988).
[14] J. Womersley, *On the oscillatory motion of a viscous liquid in thin-walled elastic tube: I.*, Phil. Mag. **46**, 199-221 (1955).
[15] M. Wibmer, *One-dimensional simulation of arterial blood flow with applications*, PhD Thesis, eingereicht an der Technischen Universitat Wien, Fakultat fur Technische Naturwissenschaften und Informatik, January, 2004.
[16] Z.Z. Wang, G. Li and O. Delestre. *Well-balanced finite difference weighted essentially non-oscillatory schemes for the blood flow model*, Int. J. Numer. Meth. Fl. **82**, 607-622 (2016).
[17] Y.L. Xing, C.W. Shu and S. Noelle, *On the advantage of well-balanced schemes for moving-water equilibria of the shallow water equations*, J. Sci. Comput. **48**, 339-349 (2011).